Electronic Supplementary Material (ESI) for Journal of Materials Chemistry A.

# Supporting Information

# $Fe^{III}$ dinuclear metallacycle complex as a size-selective adsorbent to nitrogenous compounds and potentially an effective ammonia storage

Ingrid F. Silva,[a] Ivo F. Teixeira,[b,c]* Wdeson P. Barros,[d] Carlos B. Pinheiro,[e] José D. Ardisson,[f] Gustavo M. do Nascimento,[g] Noriberto A. Pradie,[b] Ana Paula C. Teixeira,[a] and Humberto O. Stumpf.[a]*

[a] Departamento de Química, ICEx, Universidade Federal de Minas Gerais, Av. Antônio Carlos 6627, Belo Horizonte-MG, 31270-901, Brazil. E-mail: stumpf@ufmg.br

[b] Departamento de Química Fundamental, Instituto de Química, Universidade de São Paulo, Av. Lineu Prestes, 748, 05508-000 São Paulo, SP, Brazil. E-mail: ivo@iq.usp.br

[c] Departamento de Química, Universidade Federal de São Carlos – UFSCar, São Carlos, SP, Brazil.

[d] Instituto de Química, Universidade Estadual de Campinas, Campinas-SP, 13083-970, Brazil.

[e] Departamento de Física, ICEx, Universidade Federal de Minas Gerais, Belo Horizonte-MG, 31270-901, Brazil.

[f] Laboratório de Física Aplicada, Centro de Desenvolvimento e Tecnologia Nuclear (CDTN), Belo Horizonte-MG, 31270-901, Brazil.

[g] Centro de Ciências Naturais e Humanas (CCNH), Universidade Federal do ABC, Santo André-SP, 09210-580, Brazil.

**Table S1.** Summary of the crystal data and refinement conditions for **1**

| **Compound** | **1** |
|---|---|
| *Formula* | $C_{30}H_{40}Cl_6Fe_2N_4O_{16}S_4$ |
| *FW* | 1165.34 |
| *Temperature* / K | 120.0 |
| $\lambda$ / Å | 0.71703 |
| *Crystal System* | Triclinic |
| *Space group* | *P-1* |
| *a* / Å | 10.3990(3) |
| *b* / Å | 10.4057(3) |
| *c* / Å | 12.8116(4) |
| $\alpha$ / deg | 113.668(3) |
| $\beta$ / deg | 97.457(2) |
| $\gamma$ / deg | 105.922(3) |
| *Volume* / Å$^3$ | 1174.84(8) |

| | |
|---|---|
| $Z$ | 1 |
| $\rho$ / mg m$^{-3}$ | 1.647 |
| $\mu$ / mm$^{-1}$ | 1.204 |
| *F(000)* | 596.3563 |
| *Crystal size* / mm | 0.34 × 0.19 × 0.09 |
| $\theta$ / deg | 1.8 to 31.0 |
| *h k l* | $-13 \le h \le 13$; |
| | $-13 \le k \le 13$, |
| | $-17 \le l \le 17$ |
| *reflns collected* | 5317 |
| *Indep. reflns* | 5826 [$R_{int}$ = 0.032] |
| *Completeness to* $\theta$ *max(%)* | 100 |
| *Data/restraints/parameters* | 5826 / 0 / 284 |
| *GOF on* $F^2$ | 1.042 |
| $R^{[a]}$, $wR^{[b]}$ $[I > 2\sigma(I)]$ | 0.0325, 0.0837 |
| $R^{[a]}$, $wR^{[b]}$ *(all data)* | 0.0362, 0.0866 |
| *Larg. diff. peak and hole /* e Å$^{-3}$*)* | 0.88, -1.27 |

[a] $R = \Sigma ||F_o| - |F_c|| / \Sigma |F_o|$. [b] $wR = \{\Sigma[w(F_o^2 - F_c^2)^2] / \Sigma [w(F_o^2)^2]\}^{1/2}$, $w = 1/[\sigma^2(F_o^2) + (aP)^2 + bP]$ where *a,b* are adjustable constants and $P = (F_o^2 + 2F_c^2)/3$.

**Table S2.** Bond lengths for **1**.

| Bond | Length (Å) | Bond | Length (Å) |
|---|---|---|---|
| Fe1—O1 | 2.0801 (13) | N1—C7 | 1.318 (2) |
| Fe1—O4i | 2.1052 (13) | N2—C2 | 1.423 (2) |
| Fe1—O5i | 1.9829 (13) | N2—C9 | 1.317 (2) |
| Fe1—O7 | 1.9764 (14) | C2—C1 | 1.394 (2) |
| Fe1—O2 | 2.0252 (13) | C2—C3 | 1.390 (2) |
| Fe1—Cl1 | 2.2489 (5) | C9—C10 | 1.541 (2) |

| | | | |
|---|---|---|---|
| S1—O7 | 1.5356 (14) | C1—C6 | 1.384 (2) |
| S1—C11 | 1.762 (2) | C7—C8 | 1.539 (2) |
| S1—C12 | 1.768 (3) | S2—O8 | 1.5209 (14) |
| O1—C7 | 1.249 (2) | S2—C13 | 1.778 (2) |
| O4—C9 | 1.246 (2) | S2—C14 | 1.779 (2) |
| O5—C10 | 1.290 (2) | C4—C5 | 1.386 (3) |
| O3—C8 | 1.222 (2) | C4—C3 | 1.384 (3) |
| O6—C10 | 1.214 (2) | C6—C5 | 1.388 (3) |
| O2—C8 | 1.276 (2) | Cl2—C15 | 1.752 (3) |
| N1—C1 | 1.430 (2) | Cl3—C15 | 1.771 (3) |

Symetry code: (i) −x+1, −y+1, −z+2

**Table S3.** Bond angles for **1**.

| Bond | Angle (°) | Bond | Angle (°) |
|---|---|---|---|
| O4i—Fe1—O1 | 86.58 (5) | C3—C2—N2 | 120.91 (16) |
| O5i—Fe1—O1 | 89.73 (5) | C3—C2—C1 | 119.58 (16) |
| O5i—Fe1—O4i | 79.32 (5) | N2—C9—O4 | 125.64 (16) |
| O7—Fe1—O1 | 167.75 (6) | C10—C9—O4 | 117.91 (15) |
| O7—Fe1—O4i | 84.55 (6) | C10—C9—N2 | 116.44 (15) |
| O7—Fe1—O5i | 96.89 (6) | C2—C1—N1 | 119.48 (15) |
| O2—Fe1—O1 | 79.16 (5) | C6—C1—N1 | 120.26 (16) |
| O2—Fe1—O4i | 84.48 (5) | C6—C1—C2 | 120.26 (17) |
| O2—Fe1—O5i | 160.88 (5) | N1—C7—O1 | 125.27 (16) |
| O2—Fe1—O7 | 91.58 (5) | C8—C7—O1 | 118.18 (15) |
| Cl1—Fe1—O1 | 94.72 (4) | C8—C7—N1 | 116.55 (15) |

|  |  |  |  |
|---|---|---|---|
| Cl1—Fe1—O4i | 177.75 (4) | O2—C8—O3 | 128.09 (17) |
| Cl1—Fe1—O5i | 98.84 (4) | C7—C8—O3 | 119.53 (16) |
| Cl1—Fe1—O7 | 94.42 (5) | C7—C8—O2 | 112.37 (15) |
| Cl1—Fe1—O2 | 97.56 (4) | O6—C10—O5 | 128.11 (17) |
| C11—S1—O7 | 102.96 (10) | C9—C10—O5 | 112.08 (15) |
| C12—S1—O7 | 103.56 (11) | C9—C10—O6 | 119.80 (16) |
| C12—S1—C11 | 101.45 (16) | C13—S2—O8 | 104.70 (9) |
| C7—O1—Fe1 | 112.99 (11) | C14—S2—O8 | 105.58 (9) |
| C9—O4—Fe1i | 112.43 (11) | C14—S2—C13 | 97.98 (11) |
| C10—O5—Fe1i | 118.22 (11) | C3—C4—C5 | 120.28 (18) |
| S1—O7—Fe1 | 123.50 (8) | C5—C6—C1 | 119.85 (18) |
| C8—O2—Fe1 | 117.18 (11) | C6—C5—C4 | 120.01 (18) |
| C7—N1—C1 | 123.24 (15) | C4—C3—C2 | 119.98 (18) |
| C9—N2—C2 | 124.89 (15) | Cl3—C15—Cl2 | 111.51 (13) |
| C1—C2—N2 | 119.48 (15) |  |  |

Symetry code: (i) −x+1, −y+1, −z+2

The adsorption kinetics curves for this series of compounds (amines, alcohols and hydrocarbons) are shown in Figure S1. It is observed that the highest adsorption rate was found for the ammonia molecule (99.48 mmol $g^{-1}$ $h^{-1}$), followed by adsorption of the dimethylamine molecule (77.63 mmol $g^{-1}$ $h^{-1}$). The lower rates were obtained for adsorption of toluene (3.49 mmol $g^{-1}$ $h^{-1}$), followed by adsorption of aniline (3.22 mmol $g^{-1}$ $h^{-1}$) and dibutylamine (1.99 mmol $g^{-1}$ $h^{-1}$). In general, the higher the adsorption capacity of the tested compound the higher the adsorption rate of the same.

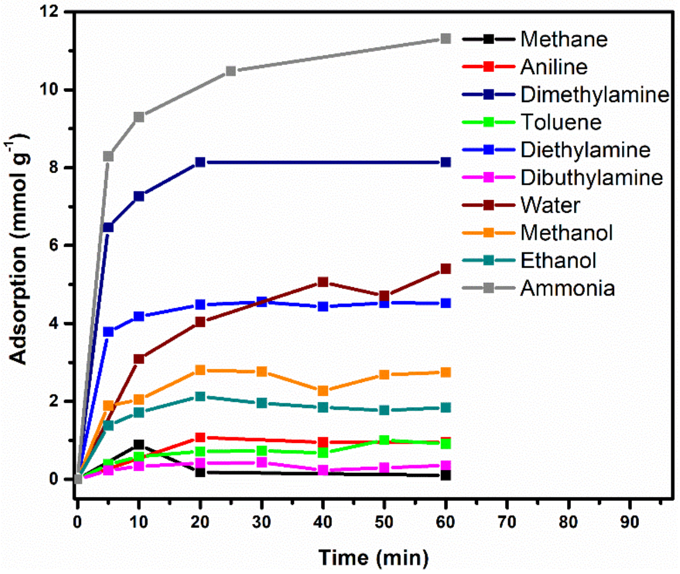

**Figure S1.** Adsorption curves, as a function of time, for a series of compounds (amines, alcohols and hydrocarbons) per gram of **1**, for one hour at 25 °C under atmospheric pressure.

Thermal gravimetric analysis of **1** and **2** were carried out in an atmosphere of synthetic air. Figures S2, S3 and S4 show the TG, DTG and DTA curves, respectively, for these compounds.

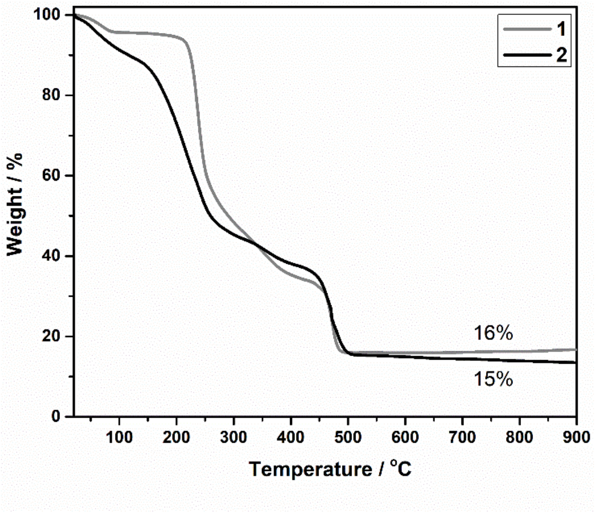

**Figure S2.** TG curves of **1** and **2** were performed in a dynamic atmosphere of synthetic air (50 mL min$^{-1}$) in an alumina crucible with a heating rate of 10 °C min$^{-1}$.

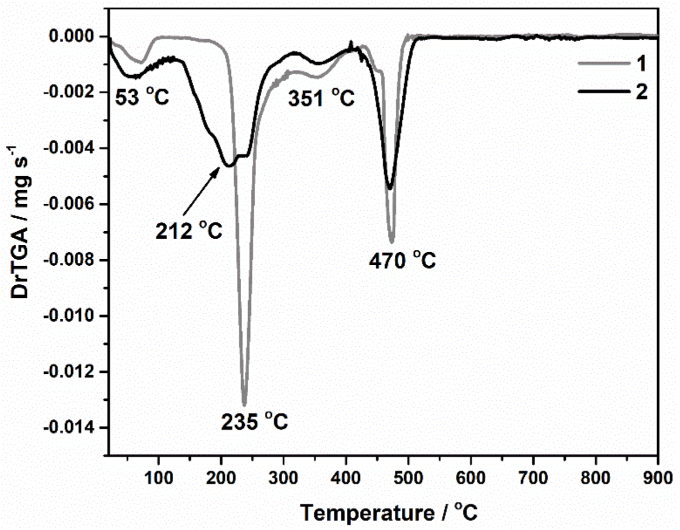

**Figure S3.** DTG curves of **1** and **2** performed in a dynamic atmosphere of synthetic air (50 mL min$^{-1}$) in alumina crucible with a heating rate of 10 °C min$^{-1}$.

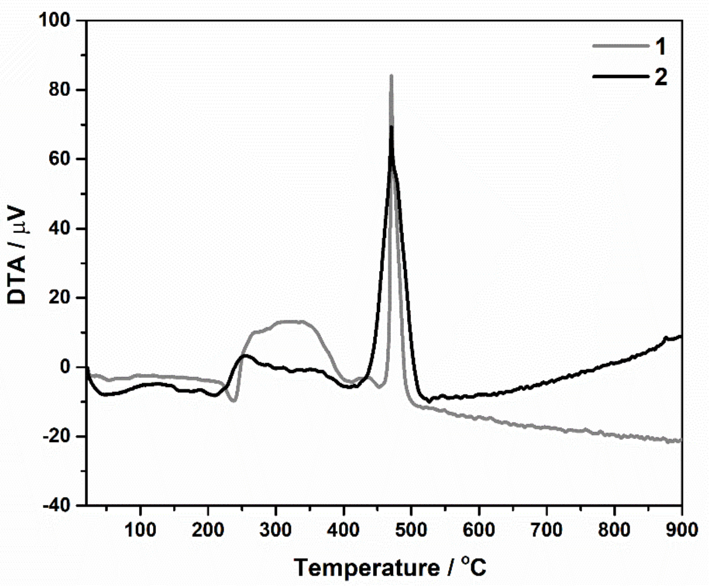

**Figure S4.** DTA curves of **1** and **2** performed in a dynamic atmosphere of synthetic air (50 mL min$^{-1}$) in an alumina crucible with a heating rate of 10 °C min$^{-1}$.

From the TGA curve obtained in air for **1**, a first loss of total mass of 3.1% can be observed in the temperature range from 22 to 90 °C, which can be attributed to the loss of two molecules of water that may be present on the surface of the structure (calculated = 3.5%). The loss of the solvents of **1** is evidenced by the endothermic event in the DTA curve (maximum peak close to 235 °C). However, in this same event was observed the partial decomposition of the complex, possibly related to the decarboxylation of the $H_2$opba ligand, due to the significant mass losses in the TG curve, to which exothermic events in the DTA curve are linked. The other losses, with maximum decomposition temperatures centered at 351 and 470 °C, may also be related to the end of the thermodecomposition of the $H_2$opba ligand and iron oxidation.[1] The experimental residue, is consistent with the analysis, approximately 15.9% (1 mol of $Fe_2O_3$ calc 15.5%).

From the TG, DTG and DTA curves of **2**, a first mass loss event was observed, with a maximum temperature centered at 53 °C, which may be related to water loss and ammonia physiosorbed. Then, by the DTG curve (Figure S3) it is observed that the second mass loss event is enlarged, in relation to the same event of **1**, starting at a lower temperature (123 °C) and ending at the same temperature as the second event curve of **1** (316 °C). The expansion of this region and the decrease in the start temperature of mass loss by the same, may be related to the loss of ammonia molecules physisorbed and chemisorbed in the structure of **2**. The temperature ranges of the other events of mass loss, referring to the decomposition of the opba ligand were the same as those observed on the TG and DTG curve of **1**. The experimental residue of the analysis, approximately 15.4%, is consistent with that expected (1 mol of $Fe_2O_3$ calc 15.0%).

The results of the CHNS and Fe atomic absorption of **1** and **2** showed a small difference between the content of the proposed C, H, N, Fe and S elements and the experimental values, Table S4. It is believed these differences occur because the compounds have a complex composition, especially due to the presence of solvent molecules. For **2** it was observed that the calculated nitrogen content is very far from the value obtained experimentally. This fact can be explained by the possible loss of the ammonia physisorbed during the measurement.

**Table S4.** Contents obtained by elemental analysis and atomic absorption of the C, H, N, Fe and S for **1** and **2**

| Compounds | Proposed formula | | %C | %H | %N | %Fe | %S |
|---|---|---|---|---|---|---|---|
| **1** | $C_{28}H_{40}Cl_2Fe_2N_4O_{18}S_4$ | Calculated | 32.60 | 3.91 | 5.43 | 10,83 | 12,43 |
| | M = 1031.49 g mol$^{-1}$ | Experimental | 32.01 | 4,10 | 5.23 | 11.18 | 13.24 |
| **2** | $C_{24}H_{68}Cl_2Fe_2N_{16}O_{16}S_2$ | Calculated | 26.60 | 6.33 | 20.68 | 10.31 | 5.92 |
| | M = 1083.62 g mol$^{-1}$ | Experimental | 27.54 | 5.56 | 9.93 | 10.71 | 7.38 |

From the data obtained by elemental analysis, atomic absorption and gravimetry for **2**, that the structure of **1** is different from **2**, which is also evidenced by colour change after ammonia adsorption, it was possible to propose a structure for this compound. The proposed structure for **2** is $[Fe_2(H_2opba)_2(NH_3)_4]Cl_2\cdot 2dmso\cdot 8NH_3\cdot 2H_2O$.

The UV-Vis absorption spectra in dmso and the diffuse reflectance spectra in the UV-Vis region for **1** and **2** are shown in Figure S5.

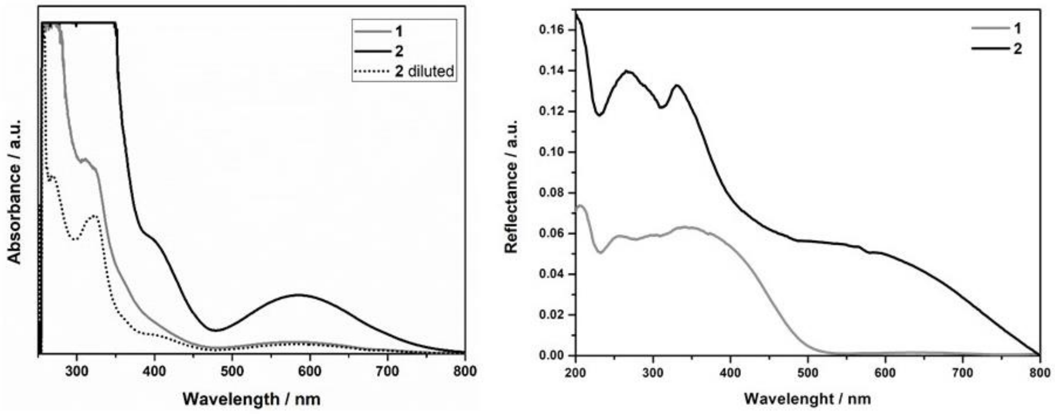

**Figure S5.** Absorption spectra in the UV region for **1** and **2**. UV-Vis spectrum of the solution in dmso (left) and diffuse reflectance spectra in the UV-Vis region (right).

Compounds **1** and **2** show quite different electron absorption spectra. The UV-Vis spectra of **2** obtained in dmso shows an intense absorption in the visible region centered at 585 nm, which gives it a bluish color, while **1** in a similar concentration shows only a small absorption. In both compounds, it is possible to observe an absorption band of higher energy at approximately 400 nm, which shows a partial conversion of **1** to **2** after ammonia adsorption. The band at 400 nm is probably related to the d-d transitions of Fe (III) and gives the yellow colour to **1**. Both compounds exhibit intense absorption in the UV region, more specifically at 320 nm associated with π-π* transitions of the opba ligand.[2]

The IR spectra obtained for the starting ligand ($H_4$opba) and for compounds **1** and **2** showed that the complex formed after the adsorption of ammonia is significantly different from the initial complex (Figure S6). It was observed, in the IR spectrum of the $H_4$opba ligand, bands at 3437 cm$^{-1}$, referring to νO-H; 3295 and 3237 cm$^{-1}$ for asymmetric and symmetrical νN-H, respectively; 1776 and 1660 cm$^{-1}$ relative to νC=O of carboxylic acids and amides, respectively; 1606 cm$^{-1}$ (νC=C); 1492 cm$^{-1}$ (δC-H); 1374 cm$^{-1}$ (δO-H); 1291 cm$^{-1}$ (δC-O); 1217 cm$^{-1}$ (νC-N); 1189 and 1177 cm$^{-1}$ (νC-O); 744 cm$^{-1}$ (δC-H out-of-plane).[3,4] The major bands of the $H_4$opba ligand spectrum were also observed in the spectrum of compound **1**. For example, the asymmetric and symmetric νN-H bands (3295 and 3237 cm$^{-1}$, respectively) were also observed in the spectrum of compound **1**, but at smaller wavenumbers (3128 and 3024 cm$^{-1}$), due to the coordination of the ligand to the metal. It was observed in the IR spectrum the bands at 1697 and 1624 cm$^{-1}$ and attributed to νC=O of carboxylates and amides, respectively;[5] 1334 cm$^{-1}$ for νC-H and bands at 1002 and 985 cm$^{-1}$ for νS=O, these last two stretches (νC-H and νS=0) are absent in the ligand spectrum, which are related to the dmso molecules present in the structure of **1**.

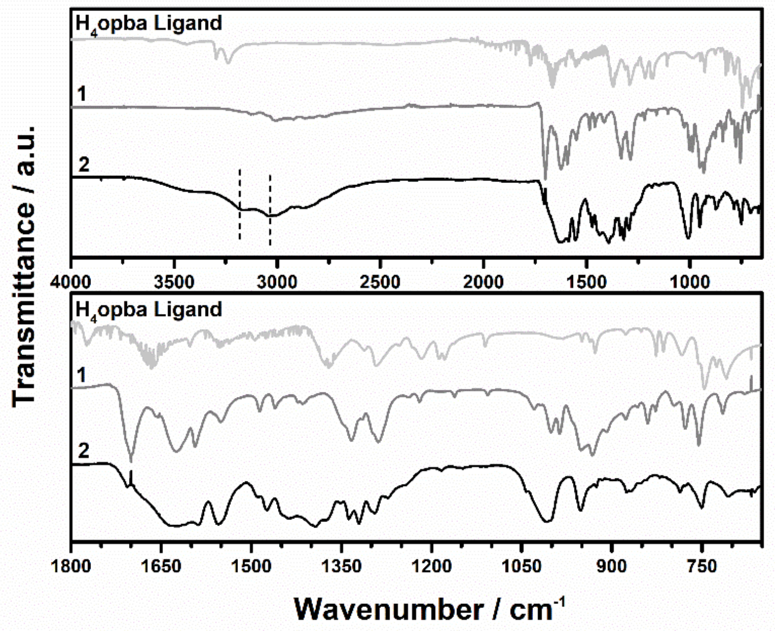

**Figure S6.** FTIR spectra for the opba ligand and compounds **1** and **2**. Below is highlighted the spectrum zoomed in the region between 1800 and 650 cm$^{-1}$.

In order to obtain a more detailed interpretation of the bands present in the high frequency region in the IR spectrum of **2** a Gaussian deconvolution was performed (Figure S7).

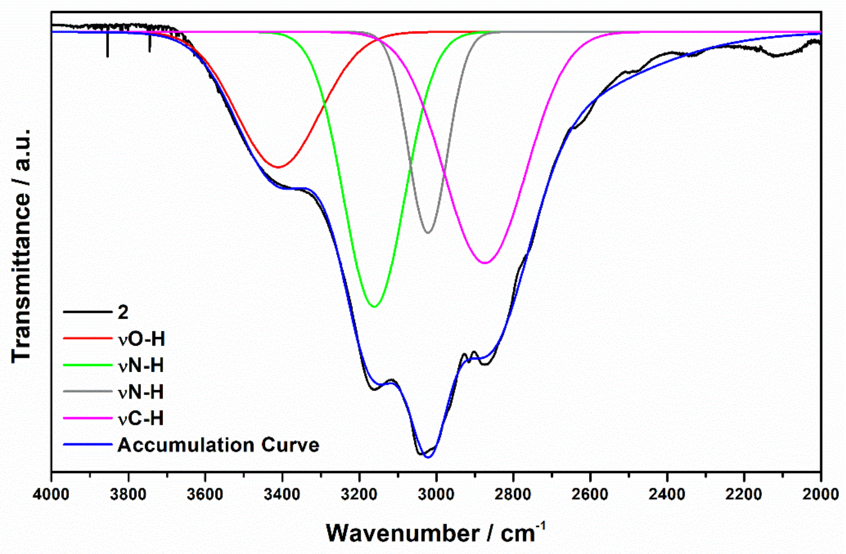

**Figure S7.** Gaussian deconvolution of the high frequency region for **2** infrared spectra.

It was observed in the IR spectra of **2** the presence of a band at 3417 cm$^{-1}$ that can be attributed to the νO-H of water molecules possibly present on the surface of the structure. The bands at 3164 and 3022 cm$^{-1}$ are related to the different νN-H present in the structure. The first and most intense band (3164 cm$^{-1}$) may be related to free $NH_3$ molecules that were only physisorbed and the band at 3022 cm$^{-1}$ can be attributed to the $NH_3$ molecules coordinated to the metal centres of **2**. The band at 2875 cm$^{-1}$ is assigned to the CH group of the dmso molecules present in **2**.[6]

The IR spectra showed that compound **2** is significantly different from **1**. Both spectra presented bands characteristic of stretches and deformations related to dmso molecules. Furthermore, for the spectrum of **2**, characteristic bands of free and coordinated ammonia were observed, indicating two different types of sorption of this molecule in the complex structure.

Figure S8 shows the Raman spectra of samples **1** and **2** at different laser lines (632.8, 785.0 and 1064.0 nm). Sample **1** has practically the same Raman spectra for different laser lines. Only at 785.0 nm, it is seen a fluorescence background between ca. 1000 to 2000 cm$^{-1}$, but the relative intensities of the Raman bands are near the same observed for the others two laser lines (632.8 and 1064.0 nm). This behaviour is in accordance to diffuse reflectance UV-Vis spectrum (Figure S5 - left) of sample **1**, which has a maximum near to 350-450 nm (or 3.54-2.75 eV). Hence, it is far from the laser energies used in the Raman experiments, precluding the resonance Raman effect. Contrarily to sample **1**, sample **2** shows Raman spectra very dependent on the laser line, in other words, sample **2** has a resonance Raman behaviour in the laser energy range investigated (from $E_{laser}$ = 1.96 eV to 1.17 eV). The changes in the Raman spectra in sample **1** after the ammonia adsorption (sample **2**) are corroborated by diffuse reflectance UV-Vis data (Figure S5 - left) of sample **2**, which has a broad absorption band from 500 to 800 nm (or 2.48-1.54 eV). These data confirm that there is an electronic interaction between the guest and the inorganic host; it indicates that at least the inorganic host chemisorbs a part of ammonia molecules. This behaviour is also corroborated by adsorption/desorption and IR data.

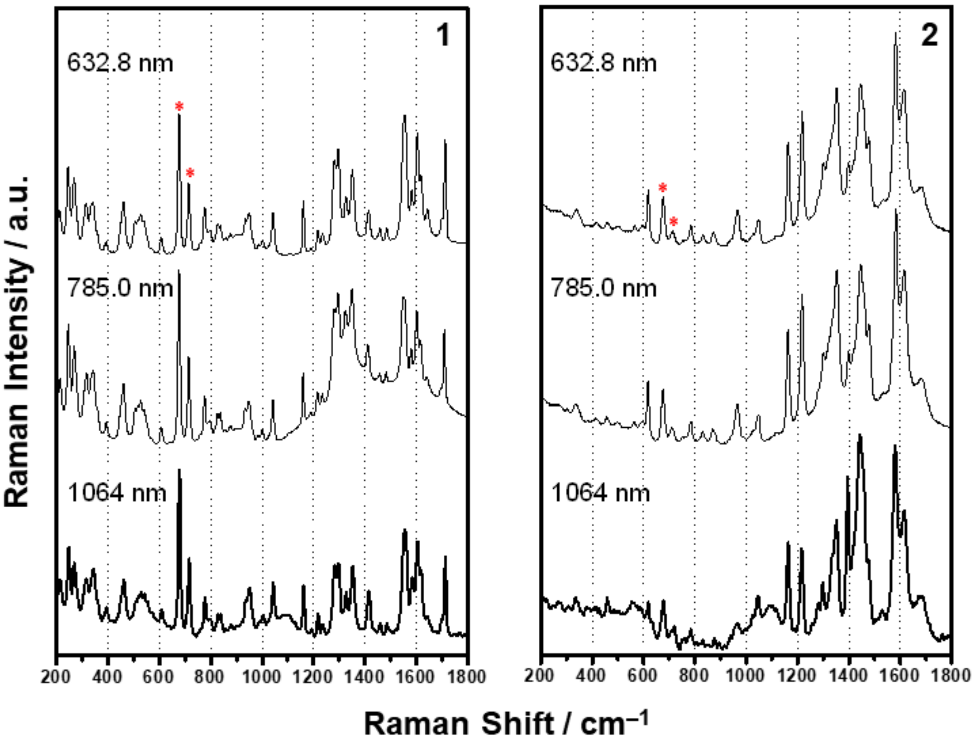

**Figure S8.** Raman spectra for the powdered samples **1** and **2** at indicated laser lines. The most intense bands assigned to dmso are indicated in the figure by (*).

The Raman spectra of sample **1** show many bands (313, 344, 678, 716, 953, 2918, 3006, and 3083 cm$^{-1}$) that can be associated to the dmso solvent present in the crystal (see complete band assignments in the Table S5). The strongest bands associated with dmso are the bands at ca. 678 and 716 cm$^{-1}$ (νC-S stretching modes).[7] These two bands associated with dmso can be used as an internal standard for measuring modifications in the relative intensities of **1** before and after ammonia adsorption. In fact, all intensities of Raman bands attributed to dmso are reduced from sample **1** to **2**. It is very interesting to notice that the bands associated to the Fe-complex from 200 to 1000 cm$^{-1}$ practically disappears after ammonia adsorption (sample **2**), however, many bands from 1000 to 1800 cm$^{-1}$ have their intensities increased. Probably, this behaviour can be associated with the resonance Raman effect associated with the formation of new chromophores after ammonia adsorption/coordination into Fe-complex. The reduction of bands from 200 to 1000 cm$^{-1}$ can be associated to the formation of a more rigid structure by ammonia adsorption, following by the elimination of torsion and out of plane vibration modes (see Table S5 for complete band assignments). The bands associated to ν(C=O) at ca. 1620, 1645, and 1714 cm$^{-1}$ have their intensities decreased (the band at 1714 cm$^{-1}$ is not observed in the compound **2**) and their values shifted from compound **1** to **2**. In addition, the increase of bands associated to aromatic rings (νC-C and νC-H) and νC-N modes can indicate that the ammonia molecules electronically interact with Fe atoms and aromatic rings from opba groups inside the cavities. Looking at the spectra of compound **2** it is clear that the Raman spectra at 632.8 and 785.0 nm are very similar in frequencies and relative intensities, but at 1064.0 nm, there are significant changes in the relative intensities of some bands. This indicates that there are two different chromophores in the compound **2**. It is important to emphasise that the same setup of bands is observed in the three laser lines (see Table S5), however, some bands have their intensities increased at 1064.0 nm. This is an interesting point; because it is not common to observe a resonance Raman, using laser line at 1064.0 nm, in fact, this trend is common in much-conjugated polymers and nanostructured carbon.[8] Maybe the incorporation of ammonia turns the composite more conjugated and the bands associated with this electronic state are intensified. Two main bands are intensified at 1064.0 nm (1394.5, 1442.5 cm$^{-1}$) and other two are observed as shoulders (1458.5 cm$^{-1}$) and with weak intensity (1529.2 cm$^{-1}$). It is important to notice that the assignment is very difficult; however, there is an indication that these bands are related to ammonia or ammonium bonded to aromatic rings and it is possible to compare with a very different system. A similar set of bands at 1409, 1444, and 1511 cm$^{-1}$ are observed when protonated aniline is adsorbed in aluminosilicates (for instance zeolite Y and montmorillonite clay).[9] These bands were associated with protonated and/or oxidized nitrogen atoms bonded to aromatic rings. Perhaps, when ammonia is incorporated to **1**, a part of the molecules bonded to aromatic rings in the opba group, and this new chemical group is Raman resonant at 1064.0 nm.

**Table S5**. Tentative assignments for Raman bands (**1**) and (**2**) samples

| Raman data | | | | | Tentative assignments |
|---|---|---|---|---|---|
| Compounds | | Literature | | | |
| **1** | **2** | $[C_4MIm]_2[Cu(opba)]$[*1] | dmso | Aniline adsorbed into ZY-Cu(II)[*4] | |
| (1064 nm) | (1064 nm) | (647.1 nm) | liquid | | |
| 213.7 | -- | *216* (**209**)[*2] | | | νFe-N out-of-plane |
| 246.3 | -- | *267* (**258**) | | | β(Fe-N-C) |
| 272.0 | -- | *290* (**281**) | | | $\beta^{\phi}$(C-H) +νFe-N |
| -- | 336.2 | *362* (**350**) | | | $\beta^{\phi}$(C-H) +νFe-N |
| 315.5 | -- | -- | 306 | | ω($SC_2$) |
| 344.0 | -- | -- | 322 | | τ($SC_2$) |

| | | | | | |
|---|---|---|---|---|---|
| 395.0 | -- | -- | 382 | | $\delta(SC_2)$ |
| 462.0 | 457.8 | *484* (**468**) | | | $\alpha$(C-H) out-of-plane |
| 531.4 | -- | *560* (**542**) | | | $\alpha$(C-H) out-of-plane |
| 543.4 | -- | *570* (**552**) | | | Ring torsion |
| 555.7 | -- | *591* (**572**) | | | Ring torsion |
| 608.7 | 617.8 | *622* (**602**) | | | Ring torsion |
| 678.4 | 676.8 | -- | 668 | | $\nu_s(SC_2)$ |
| 716.5 | 720.0 | -- | 698 | | $\nu_a(SC_2)$ |
| 777.6 | -- | *796* (**770**) | | | Ring torsion +$\nu$Fe-N |
| 800.0 | 785.0 | *832* (**805**) | | | Ring torsion out-of-plane |
| 828.5 | 831.6 | *853* (**826**) | | | Ring breathing |
| 840.8 | -- | *864* (**836**) | | | $\beta^{\phi}$(C-H) out-of-plane |
| | 871.6 | *938* (**908**) | | | $\beta^{\phi}$(C-H) out-of-plane |
| 936.6 | -- | *952* (**921**) | | | $\beta^{\phi}$(C-H) out-of-plane |
| 952.8 | -- | -- | 957 | | $\nu$(SO) +p'($CH_3$) |
| -- | 964.3 | *961* (**930**) | | | Ring torsion +$\nu$Fe-N |
| 1044.4 | 1046.3 | 1034 | | | $\beta^{\phi}$(C-H) |
| 1162.4 | 1162.6 | 1122 | | | $\beta^{\phi}$(C-H) |
| 1217.5 | 1215.6 | -- | | | $\beta^{\phi}$(C-H) |
| 1235.8 | | -- | | | $\beta^{\phi}$(C-H) |
| 1284.6 | 1279.6 | 1292 | | | $\nu$(C-N) + $\nu$(C-O) + $\beta^{\phi}$(C-H) |
| 1299 | 1297.3 | 1300 | | | $\nu^{\phi}$(C-C) + $\gamma^{\phi}$(C-H) + $\nu$(C-O) |
| 1327.4 | 1334.2 | 1333 | | | $\nu^{\phi}$(C-C) + $\gamma^{\phi}$(C-H) + $\nu$(C-N) |
| 1353.7 | 1351.2 | -- | | | -- |
| -- | 1394.5 (s) | -- | | 1409 | $\nu$(C-N)[*3] |
| 1416.9 | -- | -- | | | -- |
| -- | 1442.5 (s) | -- | | 1444 | $\nu$(C-N) |
| 1461.9 | 1458.5 (sh) | 1458 | | | $\nu^{\phi}$(C-C) + $\gamma^{\phi}$(C-H) +$\nu$(C-N) |
| 1486.1 | 1476.5 | 1473 | | | $\nu^{\phi}$(C-C) + $\gamma^{\phi}$(C-H) |
| 1557.4 | 1529.2 (w) | -- | | 1511 | $\beta$(C-N) |
| 1584.1 | 1580.2 | 1580 | | | $\nu^{\phi}$(C-C) + $\gamma^{\phi}$(C-H)[1] |
| 1606.2 | -- | -- | | | -- |
| 1620.6 | 1616.9 | 1620 | | | $\nu$(C=O) |
| 1645.2 | 1681 | 1637 | | | $\nu$(C=O) |
| 1714.3 | -- | 1669 | | | $\nu$(C=O) |

[*1] The experimental Raman band values from 1034 to 1669 for $[C_4MIm]_2[Cu(opba)]$ were collected from ref. [10] and the Raman bands for dmso molecule at liquid state were collected from ref.[7]

[*2] The band values from 961 to 216 were calculated from the equilibrium geometry of the $[Cu(opba)]^{2-}$ as described previously.[10] The band values and assignments were done based on Chemcraft visualization software and are presented in this work for the first time in order to compare with the **1**. The band values with (bold) were adjusted by the numeric factor correction of 0.9679[11] from the bands in italic. The symbol $\phi$ means that the vibrations are related to the benzene-like ring in the molecular structure of the opba group.

[*3] Bands assigned to ammonia bonded to aromatic rings into **1**. [*4] The band values were collected from ref. [9]

The magnetic properties of **1** and **2** were investigated by measuring the value of magnetization as a function of temperature ranging from 2.0 to 300 K and are shown in Figure S9, where $\chi_M$ is the molar magnetic susceptibility.

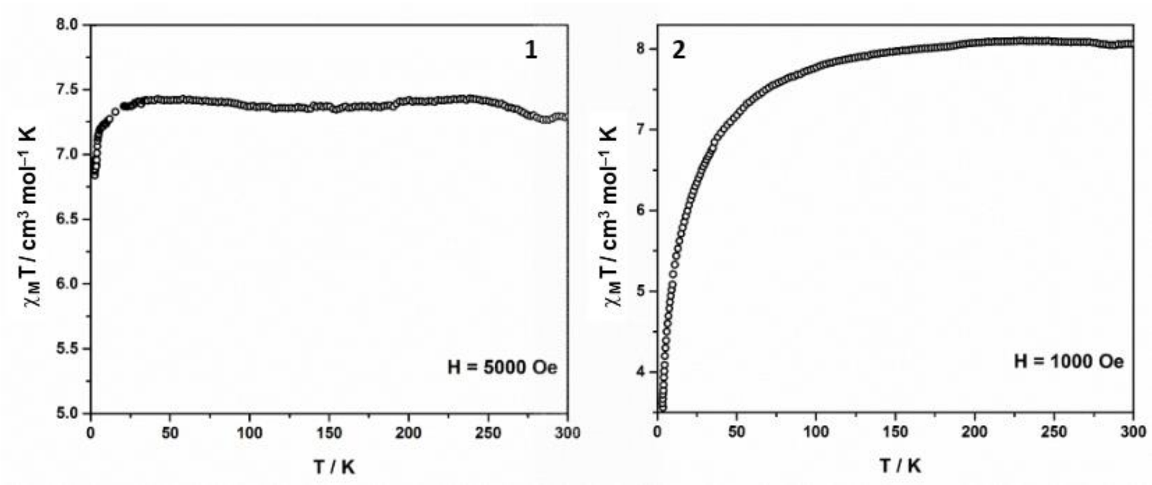

**Figure S9.** $\chi_M T$ versus T curves for compounds **1** (left) and **2** (right).

The $\chi_M T$ vs T curve for **1** (left) suggests that at room temperature there is no interaction between the spins, in other words, they are magnetically isolated. The value of $\chi_M T$ at room temperature is 7.29 cm$^3$ mol$^{-1}$ K, which is lower than the expected value for a set of two isolated iron (III) ions ($S_{Fe}$ = 5/2) in a high-spin mode [$\chi_M T_{calc}$ = 8.75 cm$^3$ mol$^{-1}$ K with $g_{Fe}$ = 2.0] .[12,13] Compound **1** behaves close to the Curie Law up to low temperature and, below 25 K, a decrease in $\chi_M T$ occurs. The shape of the curve indicates good isolation between metal ions within a dimer and even between neighboring dimers. However, at low temperatures, intermolecular interactions begin to act and, as the nature of these interactions is generally antiferromagnetic in these cases, this explains the decrease in $\chi_M T$ values.

The $\chi_M T$ values for **2** (right) remained constant from room temperature to about 100 K, in agreement with the presence of isolated spins, that is, without magnetic coupling following the Curie law. At room temperature, the product $\chi_M T$ is equivalent to 8.04 cm$^3$ mol$^{-1}$ K, a value closer to the value found for **1** for two magnetically isolated high-spin iron (III) ions (8.75 cm$^3$ mol$^{-1}$ K). The values of $\chi_M T$ exhibited a drop below 100 K reaching 3.62 cm$^3$ mol$^{-1}$ K at 3.6 K. The shape of the curve of **2** is similar to that of **1**, but the intermolecular interactions are more intense and begin to act at highest temperatures when compared to **1**.

Analyzes of the magnetic properties of **1** and **2** corroborate the existence of a change in the coordination sphere of the metal centers, since the $\chi_M T$ curve for **1** are quite different from **2**. The input of ammonia molecules, in both coordinated and solvation modes, could increase the pathways for magnetic interactions leading to more intense antiferromagnetic couplings, which is in accordance with the proposed formulas.

Magnetization measurements were also performed as a function of the applied magnetic field for **1** and **2** at 2.0 K and 4.0 K, respectively. The $M_S$ values of 2.9 (**1**) and 2.7 N$\beta$ (**2**) at 6.5 T are well below the expected values ($M_{s\ calc}$ = 10 N$\beta$ with $g_{Fe}$ = 2.0, according to the equation: $M_s = g\ S\ N\ \beta$) for a set of two non-interacting iron (III) ions ($S_{Fe}$ = 5/2) in high spin mode. This behavior is consistent to the very low intermolecular antiferromagnetic interactions between the spin carriers at low temperature, which reveals that both are more related to paramagnets.

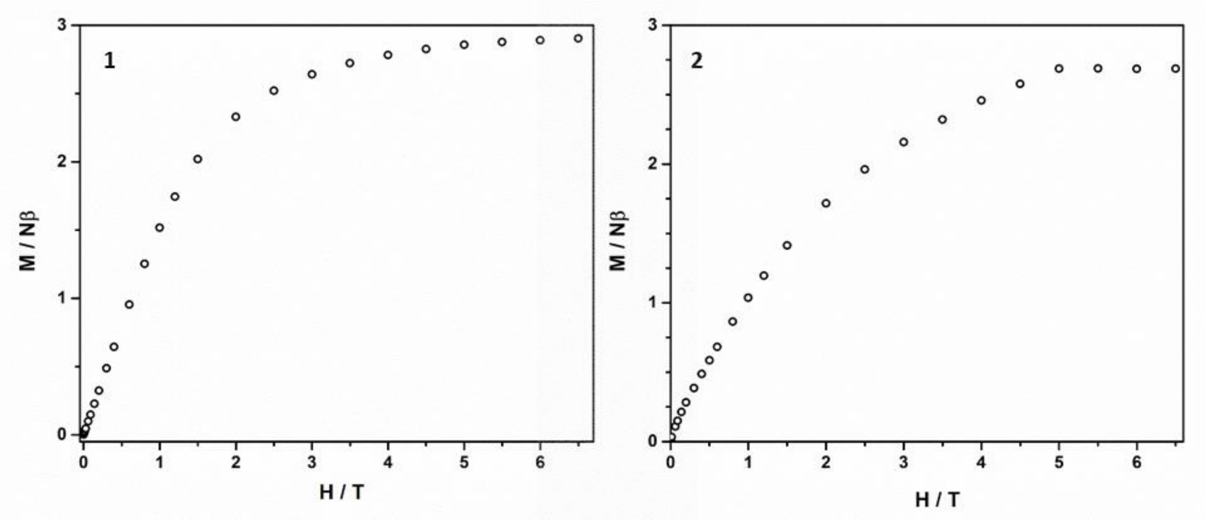

**Figure S10.** Magnetization measurement curves (M) as a function of the applied field (H) for **1** and **2** obtained at 2.0 K and 4.0 K, respectively.

It was observed that by exposing the starting material **1** in contact with ammonia, the colour changes from yellow to black within the first two minutes of adsorption. In order to better understand this transition from **1** to **2** and the role of the iron centre to the $NH_3$ adsorption, $^{57}$Fe-Mössbauer spectroscopy was performed at the temperature of 20 K of samples with 0, 2, 5, 8, 10 and 60 minutes of exposure to ammonia atmosphere (Figure S11) and their hyperfine parameters are shown in Table S5.

In the Mössbauer spectrum of the yellow solid, before being exposed to ammonia gas, it is possible to observe five different chemical environments, all with isomer shift and quadrupole splitting values typical of the $Fe^{3+}$ cation (Table S6). The hyperfine parameters of the $Fe^{3+}$ (ii) contributions are similar to the values found in the literature for the presence of iron (III) dimers and trimers directly attached to the oxygen atoms.[14–16] Thus, it is believed these chemical environments are related to the bonds of the opba ligand to iron cations. In the spectrum of **1** (T = 0 minutes) another two contributions related with $Fe^{3+}$ (i) are still observed. One of the assumptions would be that these parameters could be related to the coordination of iron with dmso and with chloride. From the Mössbauer spectra, it was observed that in the first minute of exposure to the ammonia atmosphere there is already a considerable change in the relative areas in the compound spectrum. It is observed a decrease of the areas related to the environments of $Fe^{3+}$ (i) and an increase of the areas related to the environments of $Fe^{3+}$ (ii). These relative variations continue to be observed in the material exposed to ammonia for 2 minutes. The environments of $Fe^{3+}$ (i) are no longer observed in the subsequent compounds. This decrease in chemical environments may indicate that the initial complex lost some ligands, and/or became more symmetrical.[17]

Comparing the spectra of **1** and **2** it was possible to observe that the chemical environment changes from one structure to the other, which confirms that the coordination of the complex also changes. The structure must remain an iron dimer in the black sample, possibly remaining Fe (III) and has characteristics of an octahedral geometry.

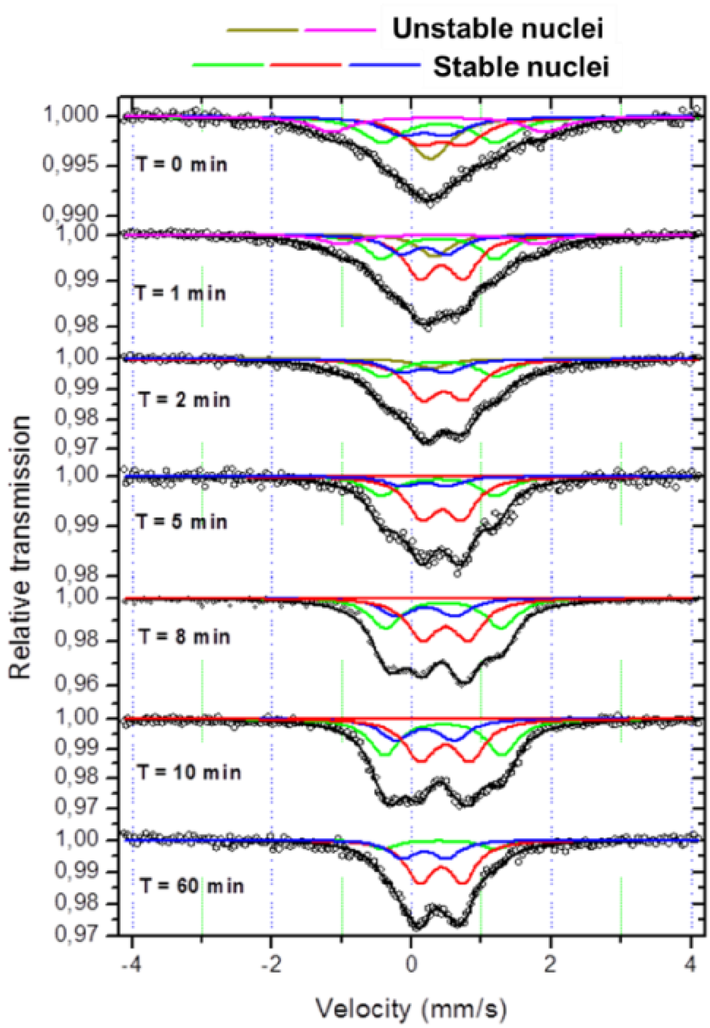

**Figure S11.** 20 K $^{57}$Fe-Mössbauer spectra obtained from samples with yellow colouring with reaction times of 0, 1, 2, 5, 8,10 and 60 minutes.

**Table S6.** Hyperfine parameters derived from the $^{57}$Fe-Mössbauer spectra of the samples with yellow colouring with reaction times of 0,1, 2, 5, 8,10 and 60 minutes

| Time (Min) | Oxidation State | δ/(mm s$^{-1}$) | ΔƐ (mm s$^{-1}$) | A (%) |
|---|---|---|---|---|
| 0 | Fe$^{+3}$ | 0.38 | - | 22 |
| | Fe$^{+3}$ | 0.48 | 1.63 | 25 |
| | Fe$^{+3}$ | 0.53 | 0.63 | 23 |
| | Fe$^{+3}$ | 0.28 | 0.65 | 16 |
| | Fe$^{+3}$ | 0.49 | 2.99 | 14 |
| 1 | Fe$^{+3}$ | 0.39 | - | 11 |
| | Fe$^{+3}$ | 0.48 | 1.59 | 22 |
| | Fe$^{+3}$ | 0.53 | 0.72 | 37 |
| | Fe$^{+3}$ | 0.28 | 0.62 | 17 |
| | Fe$^{+3}$ | 0.49 | 2.81 | 13 |

| | | | | |
|---|---|---|---|---|
| 2 | Fe$^{+3}$ | 0.38 | - | 6 |
| | Fe$^{+3}$ | 0.49 | 1.63 | 24 |
| | Fe$^{+3}$ | 0.55 | 0.61 | 48 |
| | Fe$^{+3}$ | 0.28 | 0.65 | 16 |
| | Fe$^{+3}$ | 0.49 | 2.81 | 6 |
| 5 | - | - | - | - |
| | Fe$^{+3}$ | 0.48 | 1.63 | 29 |
| | Fe$^{+3}$ | 0.53 | 0.60 | 58 |
| | Fe$^{+3}$ | 0.28 | 0.65 | 13 |
| | - | - | - | - |
| 8 | - | - | - | - |
| | Fe$^{+3}$ | 0.54 | 1.65 | 35 |
| | Fe$^{+3}$ | 0.56 | 0.66 | 45 |
| | Fe$^{+3}$ | 0.30 | 0.78 | 20 |
| | - | - | - | - |
| 10 | - | - | - | - |
| | Fe$^{+3}$ | 0.55 | 1.72 | 37 |
| | Fe$^{+3}$ | 0.57 | 0.71 | 42 |
| | Fe$^{+3}$ | 0.29 | 0.73 | 21 |
| | - | - | - | - |
| 60 | - | - | - | - |
| | Fe$^{+3}$ | 0.48 | 1.61 | 13 |
| | Fe$^{+3}$ | 0.52 | 0.62 | 61 |
| | Fe$^{+3}$ | 0.28 | 0.63 | 26 |
| | - | - | - | - |

The materials obtained after the three desorption cycles, **2**-120, **2**-160 and **2**-215, were characterized by infrared spectroscopy (Figure S12). It is observed that the FTIR spectra for the materials treated at the three temperatures are quite different. The three spectra have bands related to O-H stretches, which corroborates the desorption data indicating that the material has water molecules on the surface of its structure. The band assigned to the N-H stretch (3138 cm$^{-1}$) is quite sharp for the material **2**-120. For the other compounds (**2**-160 and **2**-215), this band practically disappears, which indicates the complete removal of the physisorbed ammonia. The band disappearance at approximately 950 cm$^{-1}$ attributed to the νS=0 in material **2**-215, which is in agreement with the others results for this compound and related to the evaporation of the uncoordinated dmso (boiling point: 190 °C) at this temperature. The assignment of the major bands of materials **2**-120, **2**-160 and **2**-215 are shown in Table S7.

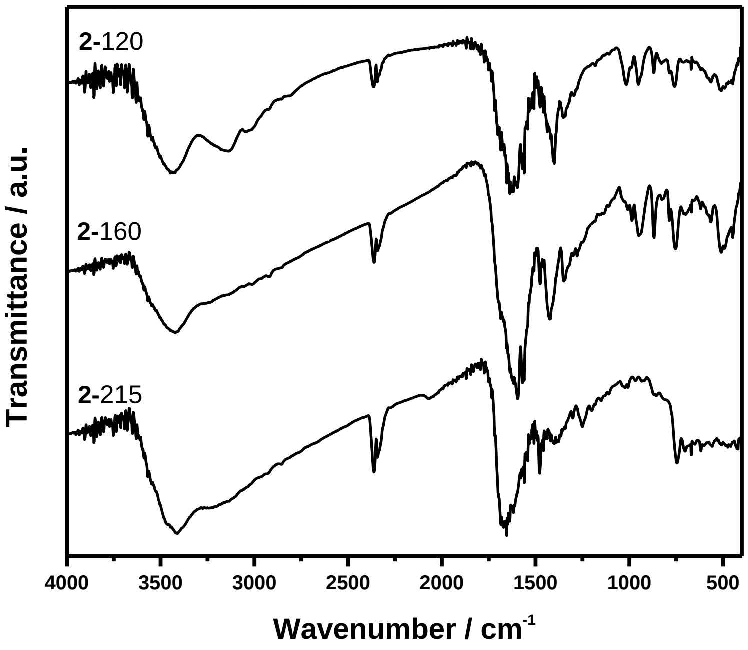

**Figure S12.** FTIR spectra for materials **2**-120, **2**-160 and **2**-215 obtained in KBr pellet.

**Table S7.** Assignment of main bands of materials **2**-120, **2**-160, **2**-215 in FTIR spectra obtained in KBr pellet

| **Assignments** | **Wavenumber / cm$^{-1}$** | | |
|---|---|---|---|
| | **2**-120 | **2**-160 | **2**-215 |
| νO–H | 3442 | 3416 | 3418 |
| νN–H | 3138 | - | 3198 |
| νC=O | 1630 | 1628 | 1674 |
| δC=C | 1598 | 1596 | - |
| δC–H | 1478 | 1478 | 1480 |
| δN–H | 1396, 1015 | 1416 | - |
| δC–H$_{\mathrm{dmso}}$ | 1352 | 1348 | - |
| νS=O | 952 | 948 | - |
| δC–H | 760 | 756, 512 | 750 |

For the three materials, **2**-120, **2**-160 and **2**-215, characteristic bands of νC=O of amides were observed, with a significant displacement of this for the material treated at 215 °C, that can be related to the partial decomposition of the $H_2opba^{2-}$

ligand, or even to the incoordination of the same. Bands related to δN-H were observed only for materials **2**-120 and **2**-160, showing that even coordinating ammonia molecules are removed in the treated compound at 215 °C.

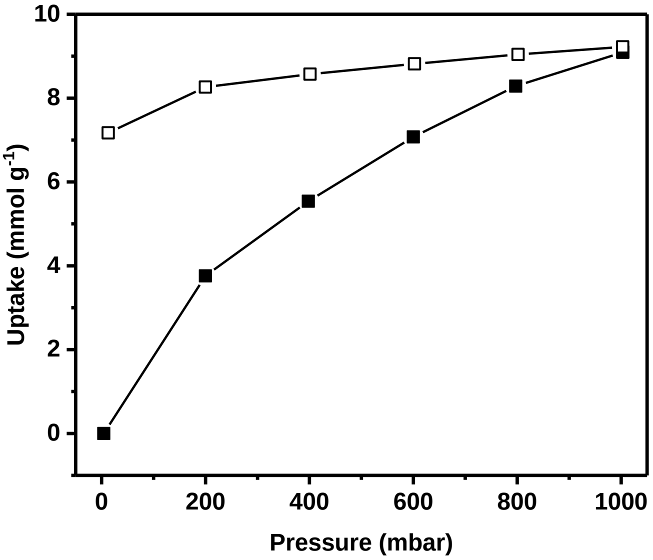

**Figure S13.** Ammonia uptake and release for the dinuclear metallacycle. Ammonia 298 K adsorption/desorption isotherm performed after a pre-treatment at 120 °C and vacuum ($10^{-3}$ Pa). Adsorption and desorption points are represented by closed and open squares, respectively.

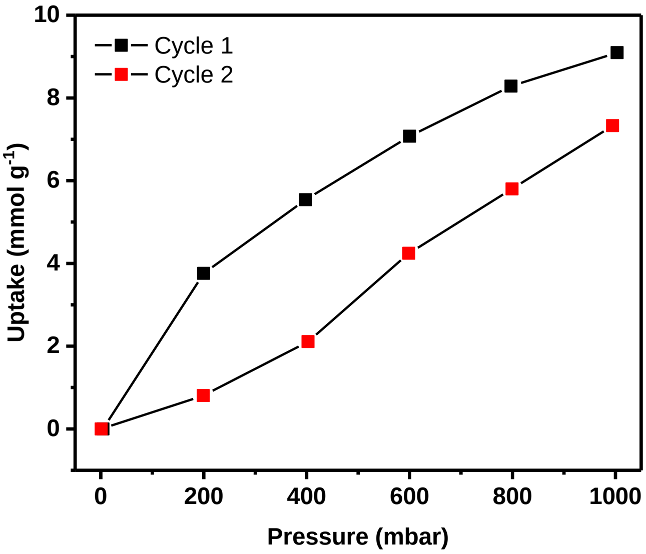

**Figure S14.** Ammonia adsorption isotherms at 298 K for the dinuclear metallacycle during consecutive cycles. The first cycle was performed without a pre-treatment at 120 °C and vacuum ($10^{-3}$ Pa). Before cycle 2 the sample was regenerated at 90 °C and $10^{-3}$ Pa.

X-ray powder diffraction experiments (XRD) were performed using a Shimadzu XRD-7000 X-Ray diffractometer using Cu filtered radiation (λ = 1.5418 Å) at room temperature in reflection mode, scanned over an angular range of 5-40° (2θ) with a step size of 1° $\text{min}^{-1}$ (2θ) and a time constant of 1s $\text{step}^{-1}$. The sample holder was submitted to a spinning speed of 60 cycles per minute to reduce any preferred orientation and to minimize rugosity effects. Figure S15 shows the values for the scattering angles (2θ) in degrees, the interplanar *d*-spacing (Å) for compounds **1** and **2.** When comparing the experimental XDR it was observed that the diffraction pattern of **2** presents few peaks, possibly related to the amorphization of the sample due to the large number of ammonia molecules present between the planes formed by the structure. This fact is corroborated by frustrated attempts at crystallization of **2**, since it was not possible to obtain monocrystals of this compound. Besides, the diffraction pattern of compound **2** is significantly different from the diffraction pattern of compound **1**, suggesting that the structure of this complex, after adsorption of ammonia is modified, although we did not have its crystalline structure.

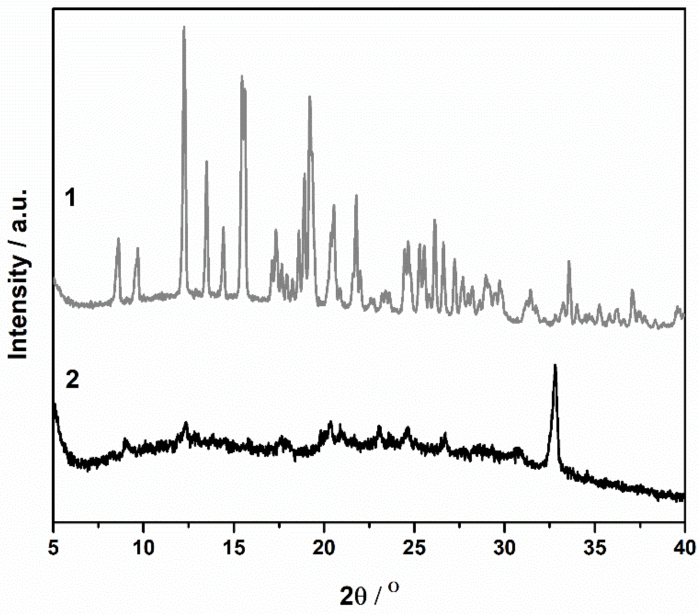

**Figure S15.** Experimental polycrystalline diffraction patterns of compounds **1** and **2**. Experimental standards were obtained using a copper tube (λ = 1.5418 Å) at room temperature.

## Notes and references

1. Keuleers, R., Janssens, J. & Desseyn, H. O. Thermal analysis of oxamates , thiooxamates and their complexes Part 2 . The Cu ( II ) complexes. **311,** 155–162 (1998).

2. Cervera, B. *et al.* Stabilization of copper(III) complexes by substituted oxamate ligands. *J. Chem. Soc. Dalt. Trans.* 781–790 (1998).

3. Tripathi, G. N. R. & Katon, J. E. Vibrational spectra and structure of qrystalline oxamic acid and sodium oxamate *. **35,** 401–407 (1979).

4. Souza, G. P. *et al.* Structural characterization of a new dioxamic acid derivative by experimental (FT-IR, NMR, and X-ray) analyses and theoretical (HF and DFT) investigations. *J. Mol. Struct.* **1016,** 13–21 (2012).

5. Simões, T. R. G. *et al.* Copper(II) assembling with bis(2-pyridylcarbonyl)amidate and N,N'-2,2-phenylenebis(oxamate). *Dalt. Trans.* **42,** 5778–5795 (2013).

6. Nakamoto, K. *Infrared and Raman Spectra of Inorganic and Coordination Compounds, Part B, Applications in Coordination, Organometallic, and Bioinorganic Chemistry*. (John Wiley & Sons, Inc., 2008).

7. Skripkin, M. Y. *et al.* Vibrational spectroscopic force field studies of dimethyl sulfoxide and hexakis(dimethyl sulfoxide)scandium(III) iodide, and crystal and solution structure of the hexakis(dimethyl sulfoxide)scandium(III) ion. *Dalt. Trans.* 4038–4049 (2004).

8. do Nascimento, G. M., Corio, P., Novickis, R. W., Temperini, M. L. A. & Dresselhaus, M. S. Synthesis and Characterization of Single-Wall-Carbon- Nanotube-Doped Emeraldine Salt and Base Polyaniline Nanocomposites. *J. Polym. Sci. Polym. Chem.* **43,** 815–822 (2005).

9. do Nascimento, G. M. & Temperini, M. L. A. Structure of polyaniline formed in different inorganic porous materials : A spectroscopic study. *Eur. Polym. J.* **44,** 3501–3511 (2008).

10. do Nascimento, G. M. *et al.* Characterization of compounds derived from copper-oxamate and imidazolium by X-ray absorption and vibrational spectroscopies. *Spectrochim. Acta Part A Mol. Biomol. Spectrosc.* **142,** 303–310 (2015).

11. Andersson, M. P. & Uvdal, P. New Scale Factors for Harmonic Vibrational Frequencies Using the B3LYP Density Functional Method with the Triple-? Basis Set 6-311+G(d,p). *J. Phys. Chem. A* **109,** 2937–2941 (2005).

12. Souza, G. P. *et al.* Synthesis and density functional calculations of the new molecule-based magnet precursor [Fe($H_2$opba-i)(dmso)$_2$]Cl. *J. Braz. Chem. Soc.* **17,** 1534–1539 (2006).

13. Pardo, E. *et al.* Chemistry and reactivity of dinuclear iron oxamate complexes: Alkane oxidation with hydrogen peroxide catalysed by an oxo-bridged diiron(III) complex with amide and carboxylate ligation. *Inorganica Chim. Acta* **357,** 2713–2720 (2004).

14. Ramos Silva, M., Coutinho, J. T., Pereira, L. C. J., Martín-Ramos, P. & Waerenborgh, J. C. Synthesis, structure and physical properties of a low dimensional compound. *Spectrochim. Acta Part A Mol. Biomol. Spectrosc.* **172,** 9–13 (2016).

15. Do, L. H., Hayashi, T., Moënne-Loccoz, P. & Lippard, S. J. Carboxylate as the protonation site in (peroxo)diiron(III) model complexes of soluble methane monooxygenase and related diiron proteins. *J. Am. Chem. Soc.* **132,** 1273–1275 (2010).

16. Dong, Y., Zang, Y., Shu, L., Wilkinson, E. C. & Que, Lawrence, J. Models for Nonheme Diiron Enzymes . Assembly of a High-Valent Fe2 (μ-O)2 Diamond Core from Its Peroxo Precursor. *J. Am. Chem. Soc.* **119,** 12683–12684 (1997).

17. Atsuchi, M., Inoue, K. & Nakashima, S. Reversible structural change of host framework triggered by desorption and adsorption of guest benzene molecules in Fe(NCS)$_2$(bpp) 2·2(benzene) (bpp = 1,3-bis(4-pyridyl)propane). *Inorganica Chim. Acta* **370,** 82–88 (2011).